Photochemical & Photobiological Sciences
https://doi.org/10.1007/s43630-026-00861-9

RESEARCH

Azure A as a promising candidate for antimicrobial photodynamic therapy of acne-related bacteria

Leandro S. Herculano[1] · Caroline T. Marcon[2] · Tânia C. S. P. Pires[3] · Cristiane Canan[4] · Mônica L. Fiorese[2] · Luis C. Malacarne[5] · André L. Tessaro[6] · Joana S. Amaral[3] · Lillian B. Barros[3]

Received: 29 October 2025 / Accepted: 20 January 2026

Abstract
Antimicrobial photodynamic inactivation (aPDT) is an effective technique for treating acne vulgaris, due to its efficiency in inactivating multiresistant bacteria and the absence of systemic side effects. This study investigated the potential of the dye Azure A (AZA), belonging to the phenothiazine class, as a photosensitizer (PS) in aPDT to combat the gram-positive bacteria *Staphylococcus epidermidis* and *Cutibacterium acnes*, both associated with inflammatory acne vulgaris. The efficiency of AZA was compared to Orthotoluidine Blue (OTB), evaluating the absorbance spectra, singlet oxygen generation rate, and minimum bactericidal concentration (MBC) at different optical fluence values and concentrations. The results demonstrated that AZA and OTB have similar spectroscopic characteristics and single oxygen generation rates, and they could inactivate both bacteria at an MBC of 0.78 μM for the smallest tested optical fluence. These findings indicate that AZA is an excellent candidate for topical aPDT applications in treating acne vulgaris and other associated infections by such bacteria.

Keywords *Staphylococcus epidermidis* · *Cutibacterium acnes* · Acne vulgaris · Phenothiazine dyes

1 Introduction

Acne vulgaris is a chronic, multifactorial inflammatory disease affecting approximately 9.4% of the global population, with a markedly higher prevalence among adolescents (85%) [1, 2]. It is characterized by inflammation of the pilosebaceous follicles, leading to purulent lesions that, in more severe cases, may extend into deeper skin layers and form painful nodules or cysts [1–3]. Although not life-threatening, acne is associated with irritation, blemishes, and scarring, often resulting in significant psychological distress, including anxiety, stress, frustration, depression, and suicidal ideation [1–5]. Its development, progression, and persistence involve multiple interacting factors, such as increased sebum production, hyperkeratinization of the pilosebaceous follicles, and the hyperproliferation of skin-resident bacteria, particularly *Cutibacterium acnes* (*C. acnes*) and *Staphylococcus epidermidis* (*S. epidermidis*)[6, 7].

The pathogenesis of acne vulgaris is governed by complex microbial interactions, with *C. acnes* acting as a key microorganism through the metabolism of sebum by lipase activity, leading to the production of propionate and free

✉ Leandro S. Herculano
leandroh@utfpr.edu.br

1 Departamento de Física, Universidade Tecnológica Federal do Paraná, Av. Brasil 4232, Medianeira, Paraná 85722-332, Brazil

2 Universidade Estadual do Oeste do Paraná, R. Guaíra 3141, Toledo, Paraná 85903-000, Brazil

3 Centro de Investigação de Montanha, SusTEC, Instituto Politécnico de Bragança, Campus de Santa Apolónia, 5300-253 Bragança, Portugal

4 Departamento de Alimentos, Universidade Tecnológica Federal do Paraná, Av. Brasil 4232, Medianeira, Paraná 85722-332, Brazil

5 Departamento de Física, Universidade Estadual de Maringá, Av. Colombo 5790, Maringá, Paraná 87020-900, Brazil

6 Departamento de Química, Universidade Tecnológica Federal do Paraná, R. Marcílio Dias 635, Apucarana, Paraná 86812-460, Brazil

Published online: 12 February 2026

fatty acids that trigger inflammatory responses [8–10]. Disease severity is closely linked to microbial dysbiosis, characterized by shifts in cutaneous phylotypes toward more pro-inflammatory lineages and a reduction in microorganisms associated with skin homeostasis and protective functions [10, 11]. In this context, *S. epidermidis*, although typically considered a commensal species, may exacerbate inflammation under conditions of microbial imbalance [10, 12]. Variations in the relative abundance of skin microbiota correlate with clinical severity [13], while biofilm formation by key species contributes to follicular obstruction and significantly increases resistance to conventional antibiotic treatments compared with planktonic cells [14, 15].

Depending on the type, stage, and chronicity of acne, current standard treatments include topical, systemic, and physical approaches that target different aspects of acne pathophysiology and are widely used in clinical practice [2, 16–33]. Despite their effectiveness, these therapies present clinically relevant limitations, including skin irritation, photosensitivity, dryness, and erythema associated with topical agents [2, 16, 17, 19], the risk of bacterial resistance linked to topical and systemic antibiotics [2, 20, 21], and significant adverse effects of systemic isotretinoin, such as teratogenicity and mucocutaneous alterations [22, 23]. Additional constraints include thromboembolic risks related to hormonal therapies [24, 25] and transient irritation caused by physical procedures like chemical peels [26–28]. Combined with poor treatment adherence and the increasing emergence of *C. acnes* resistance, these limitations have intensified interest in safer and more effective alternative treatments, particularly light-based therapeutic strategies [34].

Antimicrobial Photodynamic Therapy (aPDT) has received a significant number of studies in recent years because it does not use antibiotics or promote bacterial resistance. The aPDT is based on the interaction between light and a photosensitizer dye (PS), which results in the generation of reactive oxygen species (ROS). The interaction of the generated ROS with biomolecules, membranes, and other cellular structures induces death processes in cells and microorganisms [29–33, 35, 36].

ROS generation occurs mainly through two mechanisms. In type I reactions, the PS absorbs light, transitions to an excited triplet state (^{3}PS), and reacts with surrounding biomolecules via electron or hydrogen transfer, leading to the formation of reactive oxygen species such as superoxide, hydroxyl radicals, and hydrogen peroxide [36–39]. In type II reactions, the excited PS transfers energy directly to molecular oxygen ($^3O_2$), converting it into highly reactive singlet oxygen ($^1O_2$). Regardless of the type of mechanism, the species generated induce oxidative damage to lipids, proteins, and DNA, and excessive damage ultimately results in cell death. A schematic representation of ROS generation during aPDT is shown in Fig.1

The effectiveness of conventional aPDT is often limited by the shortcomings of first-generation PS, such as hematoporphyrin derivatives [40]. These compositions present critical challenges, including low chemical purity, long half-life in the body, and short-wavelength activation, which restricts light penetration into deeper tissues [35, 40]. In addition, organic PS may suffer from photoinstability, while the use of proprietary agents faces barriers related to oxygen dependence and the risk of resistance development [40, 41].

These general limitations are further amplified in dermatological applications, particularly in aPDT for acne treatment, where one of the main constraints is the high cost, largely associated with the photosensitizers employed. Although 5-aminolevulinic acid is approved for clinical use and applied off-label in acne therapy, its use is limited by pain during illumination, post-treatment photosensitivity, transient skin pigmentation, and high cost [31, 42]. As a result, increasing research efforts have focused on the development of more affordable, efficient, and better-tolerated photosensitizers, including curcumin [43, 44], hypericin [45], chlorophyll-a [46], indocyanine green [47], chlorin e6 [48], methylene blue [49–51], and orthotoluidine blue [52, 53].

Among the investigated compounds, phenothiazine-based dyes stand out due to their structural versatility, which allows modulation of optical absorption, solubility, membrane interactions, and phototoxicity, with reactive oxygen species generation predominantly occurring via type II photochemical mechanisms [54, 55]. In this context, phenothiazine dyes such as methylene blue (MB) and Azure B exhibit high therapeutic potential, characterized by intense absorption in the 600–800 nm spectral range and high selectivity toward tumor cells and pathogenic microorganisms [35, 56]. Despite these advantages, the broader application of this class remains limited by knowledge gaps and technical challenges, including insufficient photobiological characterization of certain derivatives and the intrinsic tendency of these molecules to aggregate in solution [56, 57]. This self-association phenomenon significantly compromises singlet oxygen generation efficiency, highlighting the need for strategies capable of stabilizing the photoactive monomeric forms [56].

Most studies addressing the use of phenothiazine dyes in aPDT have focused primarily on MB and orthotoluidine blue (OTB). In contrast, relatively few investigations have explored the potential of Azure A (AZA), despite its favorable photophysical properties. AZA exhibits a high singlet oxygen quantum yield (0.42 in water) and a high molar extinction coefficient in the red region of the visible spectrum (630 nm). Furthermore, compared to more extensively

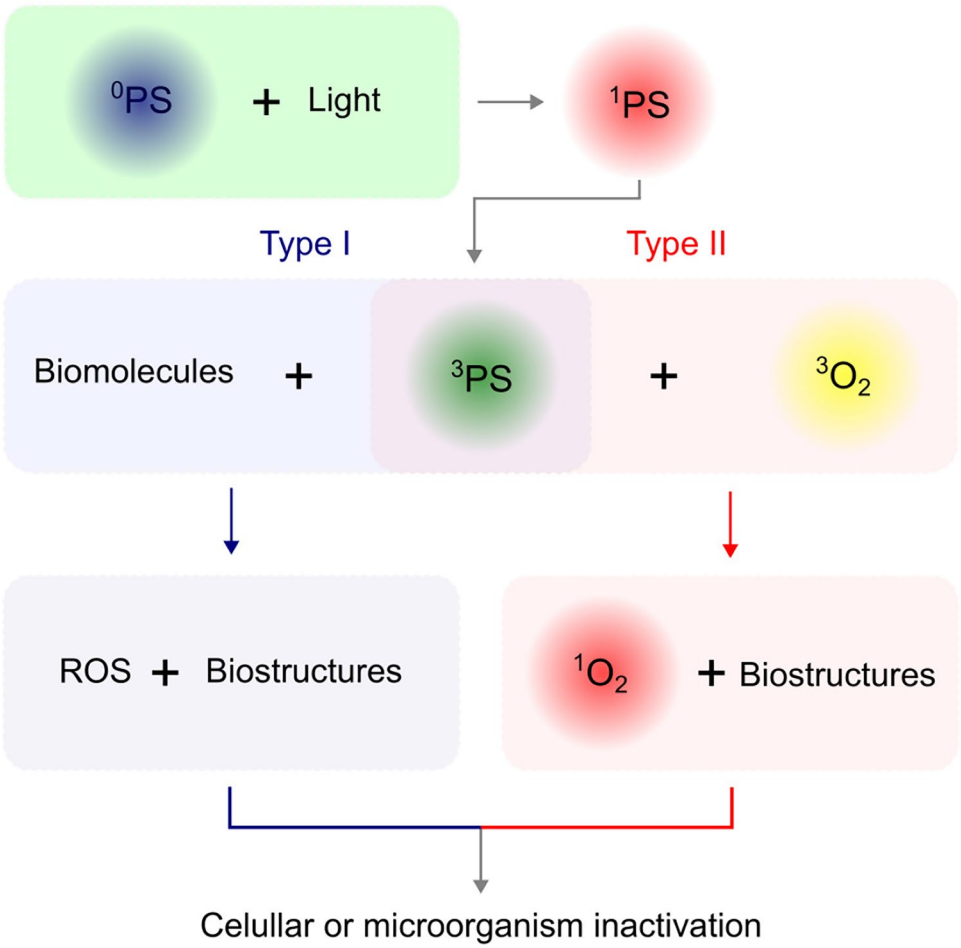

Fig. 1 PS in the ground state (^{0}PS) absorbs energy from light and undergoes a transition to the first singlet state (^{1}PS), then decays to the long-lived triplet state (^{3}PS). In the type I reaction, it interacts with biomolecules, producing ROS; in the type II reaction, it interacts with molecular oxygen in the triplet state ($^3O_2$), producing singlet oxygen ($^1O_2$). Both $^1O_2$ and other ROS interact with biostructures, causing cellular damage and death

studied phenothiazine derivatives such as MB and OTB, AZA presents a lower tendency toward self-aggregation, which contributes to preserving its ability to generate reactive oxygen species and, consequently, its photodynamic efficiency. For example, its dimerization constant at 25 °C is approximately 1,700 [58], whereas values of 2,380 for MB at 30 °C [59] and 10,500 for OTB at 25 °C [60] have been reported.

AZA demonstrates significant strategic advantages as a photosensitizer, owing to its strong interaction with mitochondrial membranes and its ability to promote photoinactivation of respiratory chain complexes even under hypoxic conditions, thereby mimicking the microenvironment of solid tumors [61]. In contrast to other phenothiazine analogs such as MB, AZA selectively inactivates mitochondrial complex IV and induces depletion of intracellular glutathione stores, weakening the antioxidant defenses of target cells [61]. Despite these favorable photodynamic properties, important limitations have been reported, particularly its dark toxicity. Acting as an uncoupler of oxidative phosphorylation, AZA reduces ATP levels and may cause systemic metabolic damage, which currently restricts its clinical application primarily to topical use or to formulations and delivery systems that markedly enhance its selectivity [61].

In parallel, recent studies have highlighted the photodynamic activity of AZA against dysfunctional mitochondria [61], reinforcing its potential for aPDT. In this context, AZA has demonstrated efficacy against a range of opportunistic fungal species, including *Candida albicans*, *Aspergillus fumigatus*, *Aspergillus niger*, *Trichoderma viride*, *Penicillium funiculosum*, and *Chaetomium globosum*. Additionally, textiles incorporating AZA into silica matrices have exhibited photodynamic activity against *Staphylococcus aureus* and *Escherichia coli*, further supporting its applicability in antimicrobial systems [62].

In the research reported here, the potential of AZA as a photosensitizer for aPDI of *S. epidermidis* and *C. acnes* bacteria was investigated. These bacteria are recognized as contributors to the maintenance and progression of inflammatory acne vulgaris. Furthermore, the results obtained were compared with those provided by OTB. For this purpose, the UV-Vis absorbance spectra, the singlet oxygen generation rate, and the Minimum bactericidal concentration

(MBC) were determined for different concentrations and optical fluences, for both dyes.

2 Materials and methods

In addition to the materials commonly used in bacterial assay routines, Azure A and Orthotoluidine Blue dyes (Sigma-Aldrich), Petri dishes containing solid medium (Columbus, Frilabo) and the bacteria strains *S. epidermidis* ATCC 12228 and *C. acnes* ATCC 11827 (Frilabo) were purchased.

2.1 Bacterial inoculum

The bacterial strains *S. epidermidis* and *C. acnes*, maintained in a nutrient medium and under refrigeration, were cultured in Petri dishes containing Columbus Agar. To ensure the viability, purity and maximum metabolic activity the bacteria were incubated anaerobically at 37 °C for 24 h. After the incubation period, immediately before the aPDI assay, a small portion of colonies of each bacterium were transferred from the Petri dishes to test tubes containing sterile water to obtain a reading of 0.5 on a McFarland densitometer (Biosan, DEN-1B), equivalent to 1.5×10^8 colony forming units per milliliter (CFU/mL). Then, 100 μL of each solution was transferred to falcon tubes and completed to 10 mL with sterile water to obtain an inoculum with approximately 10^6 CFU/mL.

2.2 UV-Vis spectroscopy

UV–Vis absorbance spectra were obtained in the range of 300–900 nm using a spectrophotometric microplate reader (SpectroStar, BMG Labtech) in order to identify the appropriate emission wavelength of the light source matching the absorbance profiles of the dyes, to allow spectroscopic comparison, and to determine for each dye the singlet oxygen generation rate. Aqueous solutions with different concentrations of the dyes (5, 17, 34, and 51 μM) were prepared and transferred to a 98-microwell plate with a flat bottom and read in the microplate reader. Furthermore, the same equipment and the same type of plate were used in the singlet oxygen generation evaluation test. Spectra were acquired in triplicate in both tests, and the results presented correspond to the averages of the values obtained, along with their respective standard deviations.

2.3 Determination of singlet oxygen generation rate

To compare the ability of dyes to generate singlet oxygen ($^1O_2$), a method based on the change in absorbance of a chemical probe when interacting with $^1O_2$ was chosen. 9,10 - Anthracenediyl - bis (methylene) dimalonic acid (ABDA) is a $^1O_2$-selective chemical probe with a conjugated aromatic system responsible for optical absorption bands observed between 360 and 400 nm. In the presence $^1O_2$, the ABDA conjugate system is broken, causing a decrease in the light absorption [63, 64]. The ABDA assay is based on the temporal monitoring of the absorbance at 380 nm of a solution containing ABDA and PS. The $^1O_2$ generated by the PS (under illumination) interacts with ABDA, promoting a decrease in absorbance at 380 nm. Assuming that the set of reactions associated with the process of breaking the conjugated system can be summarized as a pseudo-first-order kinetics, the absorbance decay of ABDA at 380 nm can be described by the equation Eq. 1 [63].

$$A_{380}(t) = A_0 e^{-k\,t}. \tag{1}$$

Here, A_0 is the initial absorbance at 380 nm ($t = 0s$), k is the decay rate of the ABDA absorbance at 380 nm and is directly related to the rate of $^1O_2$ generation by the PS.

ABDA assay was used to compare the singlet oxygen rate of both PS at different concentrations (5, 17, 34, and 51 μM) and a fixed amount of ABDA (153 μM). The solutions were illuminated in a 98-well plate by a home-developed, uniform irradiation system formed by an LED array with emission peak centered at 630 nm (described in next subsection). The assay consisted of a repetitive sequence that started with reading the absorbance spectrum (300 to 900 nm) using a microplate reader, followed by illumination of the plate for regular intervals of 30 s, from 0 to 360 s. At end, a set of absorbance spectra for both dyes was obtained. With these spectra, the absorbance values at 380 nm as a function of the illumination time were theoretically adjusted using Eq. 1 to provide the ABDA absorbance decay rates (k).

2.4 Light source

To ensure uniformity of light intensity throughout the entire illumination area of the 98-well plate, a lighting system was built based on an LED array. The system consists of a matrix of 20 LEDs evenly distributed on an aluminum printed circuit board (PCB) coupled to a forced ventilation system. The PCB-LED array is coupled to the bottow of a rectangular cross-section tube with internal walls made of mirrored acrylic plates to increase the efficiency and direct the emitted light to the upper part. At the top, a sandblasted acrylic plate with dimensions of (130 × 90) mm helps to homogenize the light distribution. All these components were joined by a box made of black acrylic plates. In addition, the intensity of de LED irradiation system(W/cm^2) was adjusted by

a microcontroller. The system was calibrated using a spectroradiometer (Gooch and Housego; OL 756) coupled to an optical fiber (Gooch and Housego, OL 730 7q-1.0) and a 50.8 mm diameter integrating sphere (Gooch & Housego, IS-270). A photograph of the system with the microplate can be seen in Fig. 2, step 8.

2.5 Antimicrobial photodynamic inactivation assay

The main objective was to verify AZA dye's effectiveness as a possible PS for the photodynamic inactivation of bacteria associated with acne vulgaris and compare it with OTB, a well-known PS used in aPDT assays. For this purpose, the aPDT assay was adapted to determine the minimum bactericidal concentration (MBC) of both PS when subjected to illumination under different optical fluence. In this case, no colony counting process was necessary. The series of steps that make up the aPDT assay can be schematically described by the sequence shown in Fig. 2.

Preliminarily, bacterial inocula were prepared to obtain strains of *S. epidermidis* and *C. acnes* with 10^6 CFU/mL in sterile water. Following, 150 μL of sterile water to lines B to H and columns 1 to 6 of the 98-well plate (Fig. 2, step 2). After that, 150 μL of the 500 μM solution of the PS were added to the wells of lines A and B, with AZA being pipetted

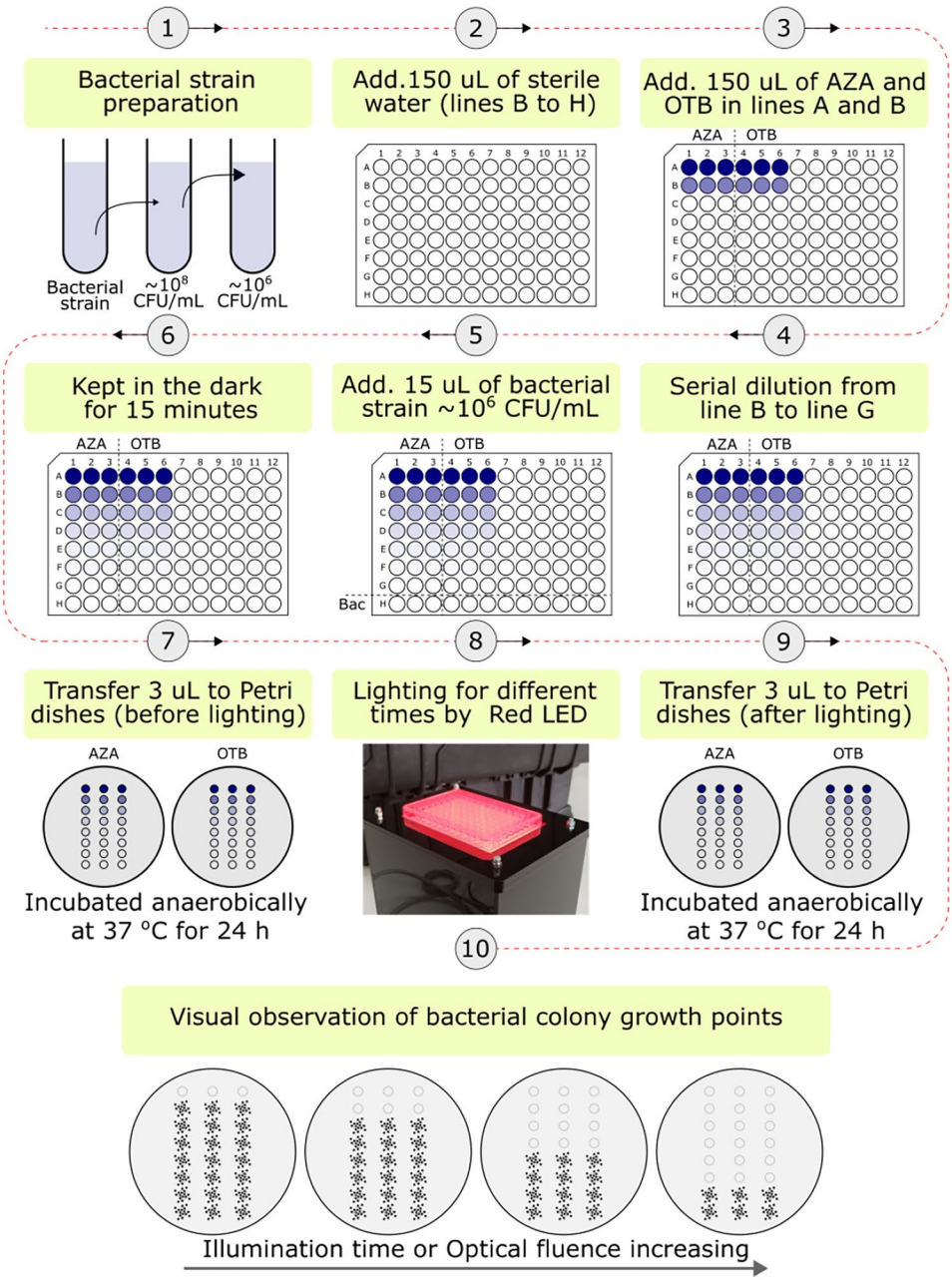

Fig. 2 In vitro aPDT assay steps: (1) inoculum preparation, (2-6) microplate preparation, (7) dark control - transfer of 3 μL aliquots from each well before the illumination process, (8) illumination, (9) transfer of 3 μL aliquots from each well after the illumination process and (10) observation of the absence/presence of bacterial growth

into columns 1 to 3 and OTB into columns 4 to 6 (Fig. 2, step 3).

The serial dilution was performed starting with the transfer of 150 μL from the wells of line B to line C and homogenization until the wells of line G. The line H is leaving without PS to be used as a control and to check the possible effects of light on the multiplication of bacteria (Fig. 2, step 4). Next, 15 μL of bacterial inoculum is added to each well, resulting in approximately 10^5 CFU/mL (Fig. 2, step 5). After inoculating the bacteria, the 98-well plate is kept in the dark for 15 min to allow interaction between the PS and the bacteria (Fig. 2, step 6).

To evaluate the antimicrobial activity generated by the PS in the absence of light, after the interaction period, using an 8-channel micropipette, 3 μL from each well are transferred to two Petri dishes (one for lines 1 to 3 and another for lines 4 to 6) containing solid PCA agar medium. An arrow marked on the bottom indicates the direction of increasing concentration and the name of the PS (Fig. 2, step 7). The plates are kept half-open inside the Laminar flow cabinet to dry the liquid for subsequent incubation at 37 °C for 24 h.

In the illumination process, the same 98-well plate was placed on the light system for 20 min (Fig.2, step 8). Then, the process of transferring 3 μL from each well to new Petri dishes, drying, and incubation at 37 °C for 24 h was repeated (Fig. 2, step 9). The same plate was again subjected to illumination for 20 min and transferred to a Petri dish two more times. These procedures resulted in four Petri dishes for each PS, with illumination times of 0, 10, 20, and 40 min, corresponding to an optical fluency of 0, 12, 25 and 50 J/cm^2. This process was performed separately for each bacteria.

After the incubation period, the results were analyzed by checking, for each Petri dish with a given illumination time, the pipetting point corresponding to the lowest concentration that did not present bacterial growth (Fig. 2, step 10). The Petri dishes were photographed and organized in a vector graphics editing program (Inkscape). Repeating the pipetting process on lines 1-3 and 4-6 ensures the procedure is performed in triplicate for both PS.

3 Results

3.1 Spectral characterization

Figure 3 shows the absorbance spectra obtained for the aqueous solutions of OTB (Fig. 3a) and AZA (Fig. 3c) at concentrations of 5, 17, 34, and 51 μM.

In both cases, the spectra exhibit a predominant absorption band centered around 630 nm and a shoulder near 590 nm, which is more evident for AZA, both features being characteristic of monomeric species [58, 60]. The linear relationship between the maximum absorption value at 628 nm for OTB and 635 nm for AZA as a function of concentration is shown in Fig. 3b and d, respectively. Linear fitting yields rates of change in absorbance with concentration of $\beta_{\mathrm{OTB}} = (37 \pm 5) \times 10^{-3}\ \mu\mathrm{M}^{-1}$ for OTB and $\beta_{\mathrm{AZA}} = (33 \pm 1) \times 10^{-3}\ \mu\mathrm{M}^{-1}$ for AZA.

To further assess the aggregation state, the ratio between the absorbance at 590 nm and the main monomeric absorption band (628 nm for OTB and 635 nm for AZA) was evaluated, as shown in Fig. 3e. This analysis indicates that both dyes remain predominantly in their monomeric form up to a concentration of 17 μM, above which partial dimerization is observed.

3.2 Singlet oxygen generation rate

Figure 4 presents the absorbance spectra of AZA (Fig. 4a, blue curve) and OTB (Fig. 4b, blue curve), together with the normalized emission spectrum of the light source (Fig. 4, red curves). In both cases, a strong spectral overlap between the emission of the light source and the absorption bands of the photosensitizers is observed. The emission spectrum of the source exhibits a peak at 630 nm, coinciding with the absorption maxima of both PS.

The assay used to determine the singlet oxygen ($^1O_2$) generation rate is based on monitoring the decay of the ABDA absorbance at 380 nm under irradiation in the presence of a PS. Figure 4a shows the absorbance spectra of AZA at 17 μM in the absence (blue curve) and presence (black curve) of 153 μM ABDA. A similar analysis was performed for OTB, whose absorbance spectra at 17 μM without ABDA (blue curve) and with 153 μM ABDA (black curve) are shown in Fig. 4b. No significant spectral overlap between the PS and ABDA is observed in the region of interest. At 380 nm, the absorbance of ABDA is approximately 14 times higher than that of the PS.

Figure 5 presents the absorbance spectra, in the 300–800 nm range, of aqueous solutions containing ABDA (153 μM) and different concentrations of AZA under illumination times ranging from 0 to 360 s. From these spectra, the absorbance values at 380 nm were extracted for each illumination interval, yielding the corresponding decay curves of ABDA absorbance in the presence of AZA. An analogous procedure was performed for OTB, as shown in Fig. 6.

For all investigated photosensitizer concentrations, the temporal evolution of the absorbance spectra (Fig. 5a,c,e,g for AZA and Fig. 6a,c,e for OTB) shows a progressive decrease in the absorbance of ABDA in the region around 380 nm as a function of irradiation time. No significant changes in the absorbance bands of the photosensitizers are observed during illumination.

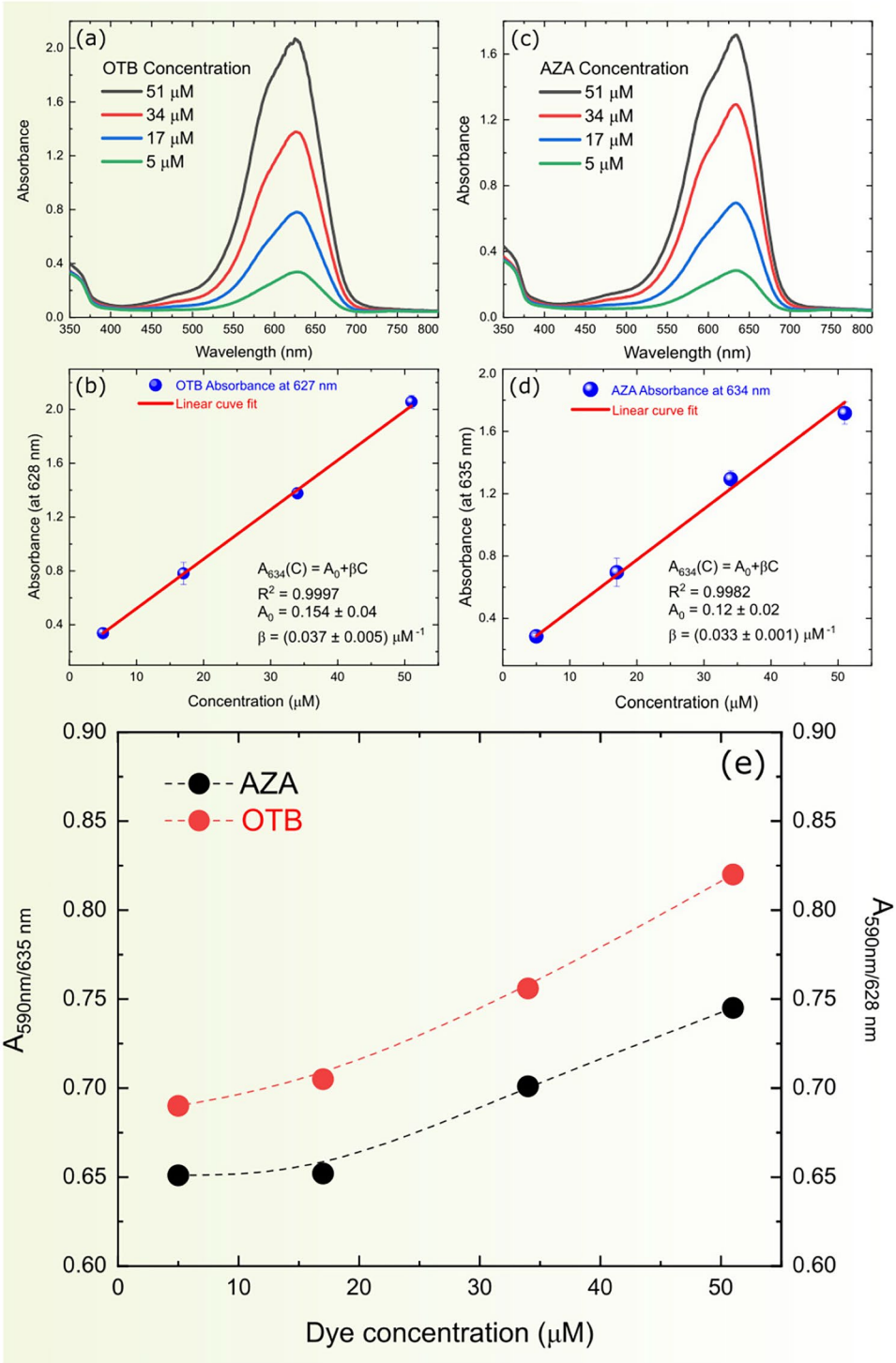

Fig. 3 Absorbance spectra in the region of interest from 300 to 850 nm for 5, 17, 31, and 51 μM concentrations of the dyes (a) OTB and (c) AZA. Absorbance values at the peak wavelengths of the dyes (b) OTB (627 nm) and (d) AZA (634 nm) and linear fit (red colored line) describing the linear relationship between the absorbance and the concentrations of the dyes. (e) Ratio between the absorbance at 590 nm (corresponding to the dimeric species) and the main monomeric absorption band (628 nm for OTB and 635 nm for AZA)

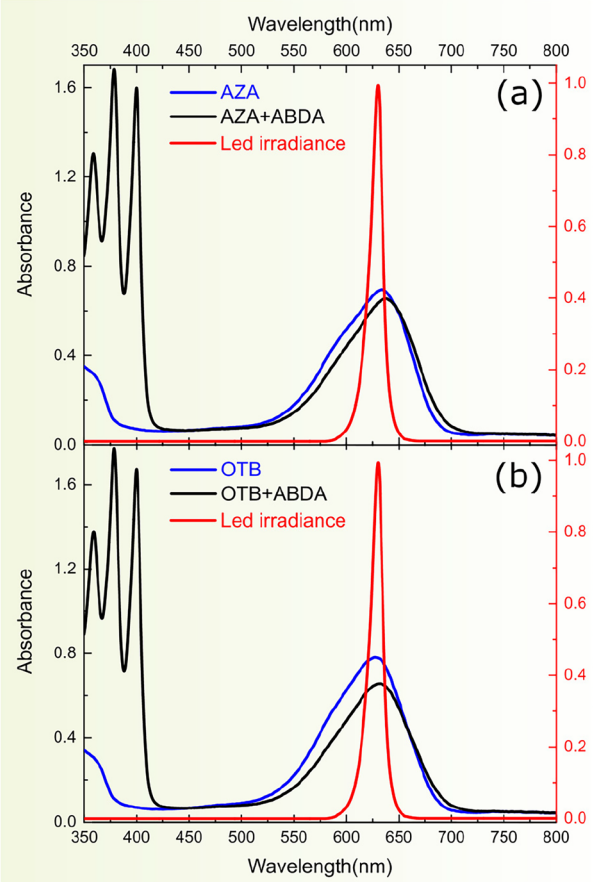

Fig. 4 Absorbance spectra of the aqueous solution containing (a) 17 μM AZA (blue curve) and 17 μM AZA and 153 μM ABDA (black curve). Absorbance spectra of the aqueous solution containing (b) 17 μM of OTB (blue curve) and 17 μM OTB and 153 μM ABDA (black curve). The red continuous lines represents the normalized irradiation spectra of light source (red LED)

By fitting the decay of the absorbance at 380 nm using Eq. 1, the decay rates of ABDA were determined for different photosensitizer concentrations. The resulting decay rates as a function of PS concentration are presented in Fig. 7. Both AZA and OTB exhibit similar decay rate values over the investigated concentration range. In addition, for both photosensitizers, a tendency toward saturation is observed for concentrations above approximately 34 μM.

3.3 Efficacy of in vitro aPDT

The antimicrobial photodynamic therapy (aPDT) assay consisted of exposing bacterial inocula containing different concentrations of photosensitizers to varying light exposure times. After irradiation, aliquots of each inoculum were transferred, in triplicate, to Petri dishes containing solid culture medium. Following incubation at 37 °C for 24 h, the presence or absence of visible bacterial colonies at the pipetting points was evaluated. The minimum bactericidal concentration (MBC) for each photosensitizer and irradiation time was defined as the lowest PS concentration at which no visible bacterial growth was observed.

Figures 8 and 9 present representative photographs of the Petri dishes containing inocula of *C. acnes* and *S. epidermidis*, respectively, treated with different concentrations of AZA and OTB and exposed to different optical fluence values. In the dark control experiments (Fig. 8a and e), corresponding to inocula not exposed to light, visible growth of *C. acnes* was observed at all pipetting points for both AZA and OTB across the investigated concentration range (0–50.00 μM).

Figure 8b, c, d, f, g, and h show the photographs of the Petri dishes that received aliquots from the 98-well plate after different illumination times. In these images, pipetting points without visible growth of *C. acnes* can be observed. Since each pipetting point corresponds to a different photosensitizer concentration, the images indicate that increasing optical fluence, achieved by longer illumination times, is associated with a reduction in the minimum bactericidal concentration (MBC).

According to the photographs shown in Fig. 8, for the lowest and highest optical fluence values investigated (12 J/cm^2 and 50 J/cm^2), the MBC values for *C. acnes* were 6.25 μM and 0.78 μM, respectively, for both AZA and OTB. Additionally, growth was observed at all pipetting points corresponding to wells that did not contain photosensitizer (line H) but were exposed to light, indicating the absence of bactericidal effects due to light alone.

Similar results were obtained for the aPDT assay performed with *S. epidermidis*, as shown in Fig. 9. In the dark control experiments (Fig. 9a and Fig. 9e), bacterial growth was observed at all pipetting points for the entire concentration range tested (0.78–50 μM). In contrast, for the plates corresponding to different optical fluence values (Fig. 9b, c, d, f, g, and h), several pipetting points without bacterial growth were observed, indicating bacterial inactivation.

For AZA, the MBC values for *S. epidermidis* at the lowest and highest optical fluence values (12 J/cm^2 and 50 J/cm^2) were 3.13 μM and 0.78 μM, respectively. For OTB, the corresponding MBC values were 12.5 μM and 1.56 μM. Growth was observed at all pipetting points corresponding to wells without photosensitizer but exposed to light.

Table 1 summarizes the MBC values obtained in the aPDT assays for both bacteria treated with AZA and OTB under different optical fluence conditions.

As observed in Figs. 8 and 9 and summarized in Table 1, it was possible to note that AZA, within the range of optical fluence and concentration values investigated, presents at least the same photodynamic inactivation capacity as OTB for *C. acnes* and presents MBC for *S. epidermidis* equal to

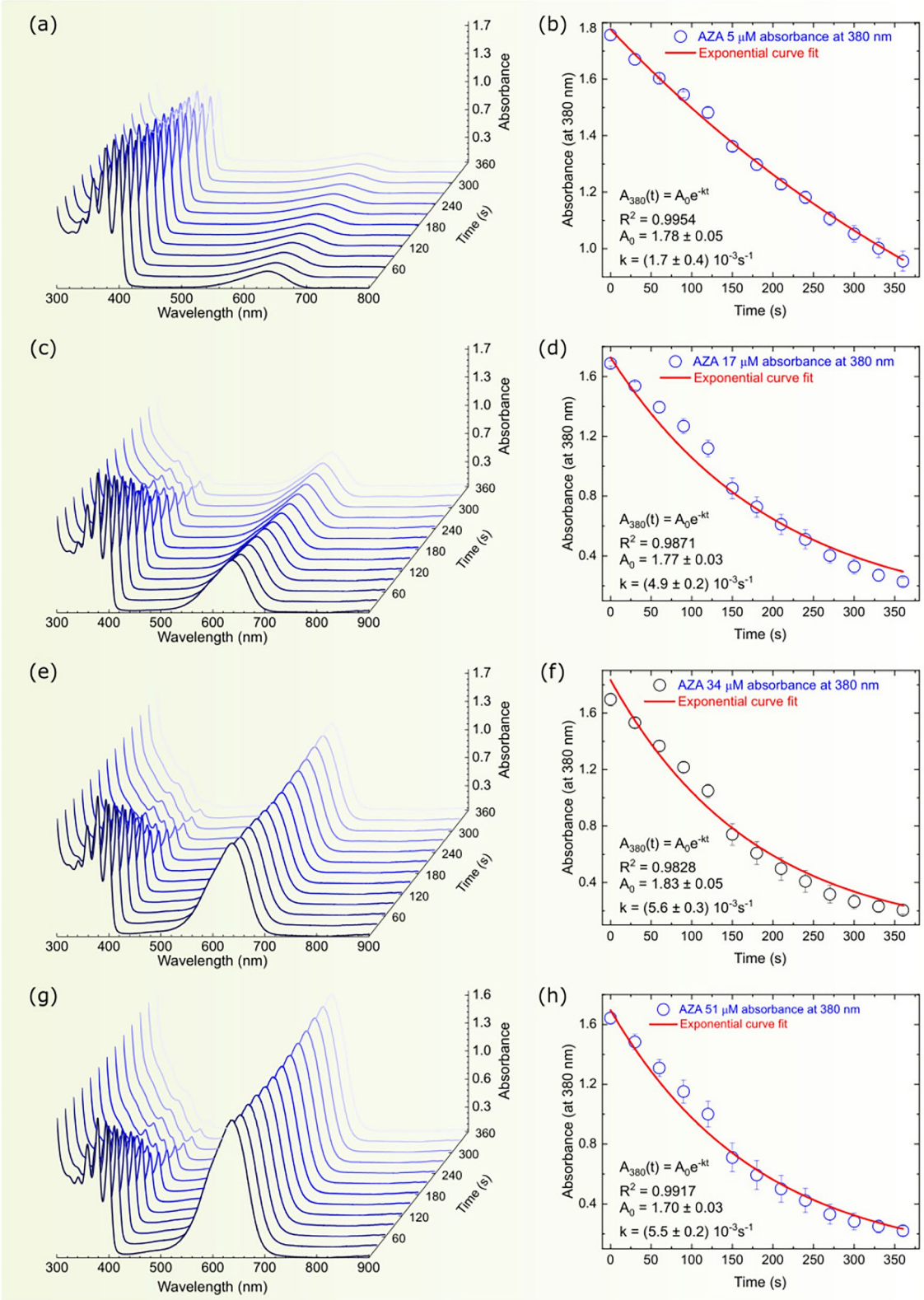

Fig. 5 Absorbance spectra in the region of interest (300 to 800 nm) of the aqueous solution of ABDA (153 μM) as a function of exposure time to light (630 nm) containing different concentrations of AZA: (a) 5 μM, (c) 17 μM, (e) 34 μM, and (g) 50 μM. Absorbance measured at 380 nm as a function of exposure time to light of the AZA solution: (b) 5 μM, (d) 17 μM, (f) 34 μM, and (h) 50 μM. The red curve represents the theoretical fit using Eq. 1

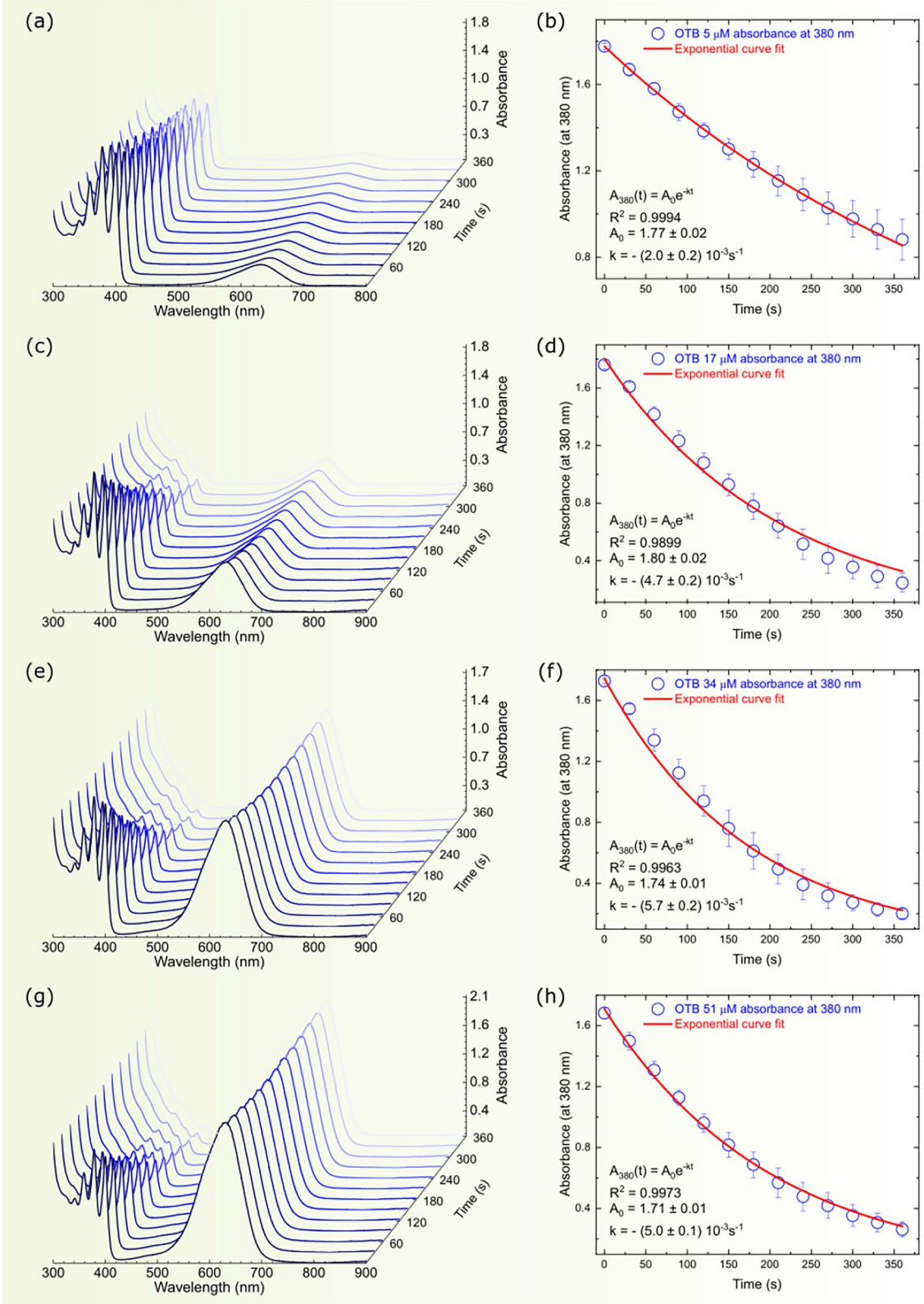

Fig. 6 Absorbance spectra in the region of interest (300 to 800 nm) of the aqueous solution of ABDA (153 μM) as a function of exposure time to light (630 nm) containing different concentrations of OTB: (a) 5 μM, (c) 17 μM, (e) 34 μM, and (g) 50 μM. Absorbance measured at 380 nm as a function of exposure time to light of the OTB solution: (b) 5 μM, (d) 17 μM, (f) 34 μM, and (h) 50 μM. The red curve represents the theoretical fit using Eq. 1

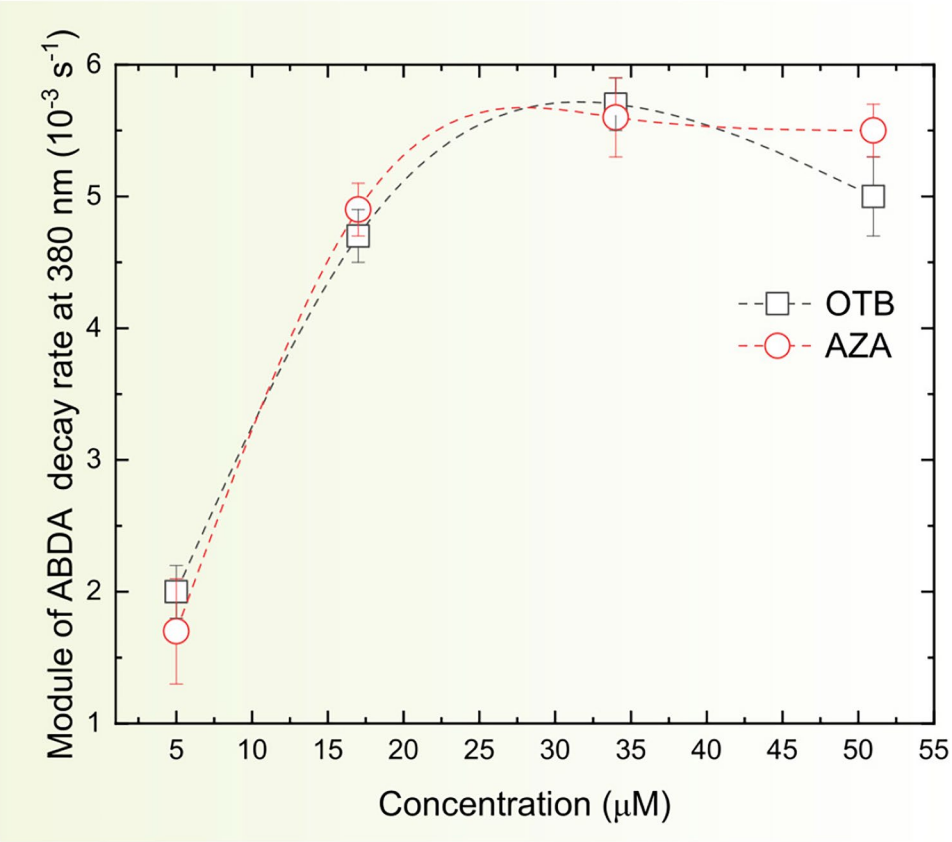

Fig. 7 The decay rate for the ABDA oxidation for different AZA (circles) and OTB (squares) concentrations. The dashed line is only a visual guide

half the value obtained when using OTB, a PS already studied for aPDT [52, 53], demonstrating the potential of AZA to be used as a PS for the photodynamic treatment of acne vulgaris. As mentioned, AZA has the advantage of a lower tendency to self-aggregate in water.

4 Discussion

4.1 Spectral characterization

The statistically similar values of β obtained for OTB and AZA indicate comparable optical behavior, despite the presence of different substituent groups in their molecular structures. This similarity is consistent with the absorption spectra shown in Fig. 3a and c, which display analogous spectral profiles for both dyes. Such behavior is expected, since both photosensitizers share the phenothiazine core, which is responsible for optical absorption in the visible region [54, 55, 65].

The linear dependence of absorbance on concentration, illustrated in Fig. 3b and d, further supports the interpretation that both dyes remain predominantly in their monomeric state within the investigated concentration range. This conclusion is corroborated by the absorption spectra, which exhibit a dominant monomeric band around 630 nm and only a weak shoulder near 590 nm, typically associated with dimeric species.

A more definitive assessment of aggregation effects is provided by the absorbance ratio analysis shown in Fig. 3e. The nearly constant ratio observed up to 17 μM indicates minimal contribution from dimeric species, whereas deviations at higher concentrations reveal the onset of partial dimerization. Together, the spectral features and quantitative analysis confirm that monomeric absorption dominates at low concentrations, with aggregation becoming relevant only beyond this threshold.

4.2 Singlet oxygen generation rate

The strong overlap between the emission spectrum of the light source and the absorption spectra of both photosensitizers, as shown in Fig. 4, ensures efficient excitation at 630 nm. This spectral matching maximizes photon absorption by the PS and is therefore expected to enhance the production of reactive oxygen species (ROS). In the context of antimicrobial photodynamic therapy (aPDT), such selective activation is particularly advantageous, as it minimizes losses due to inefficient excitation and reduces potential phototoxic effects on non-target tissues.

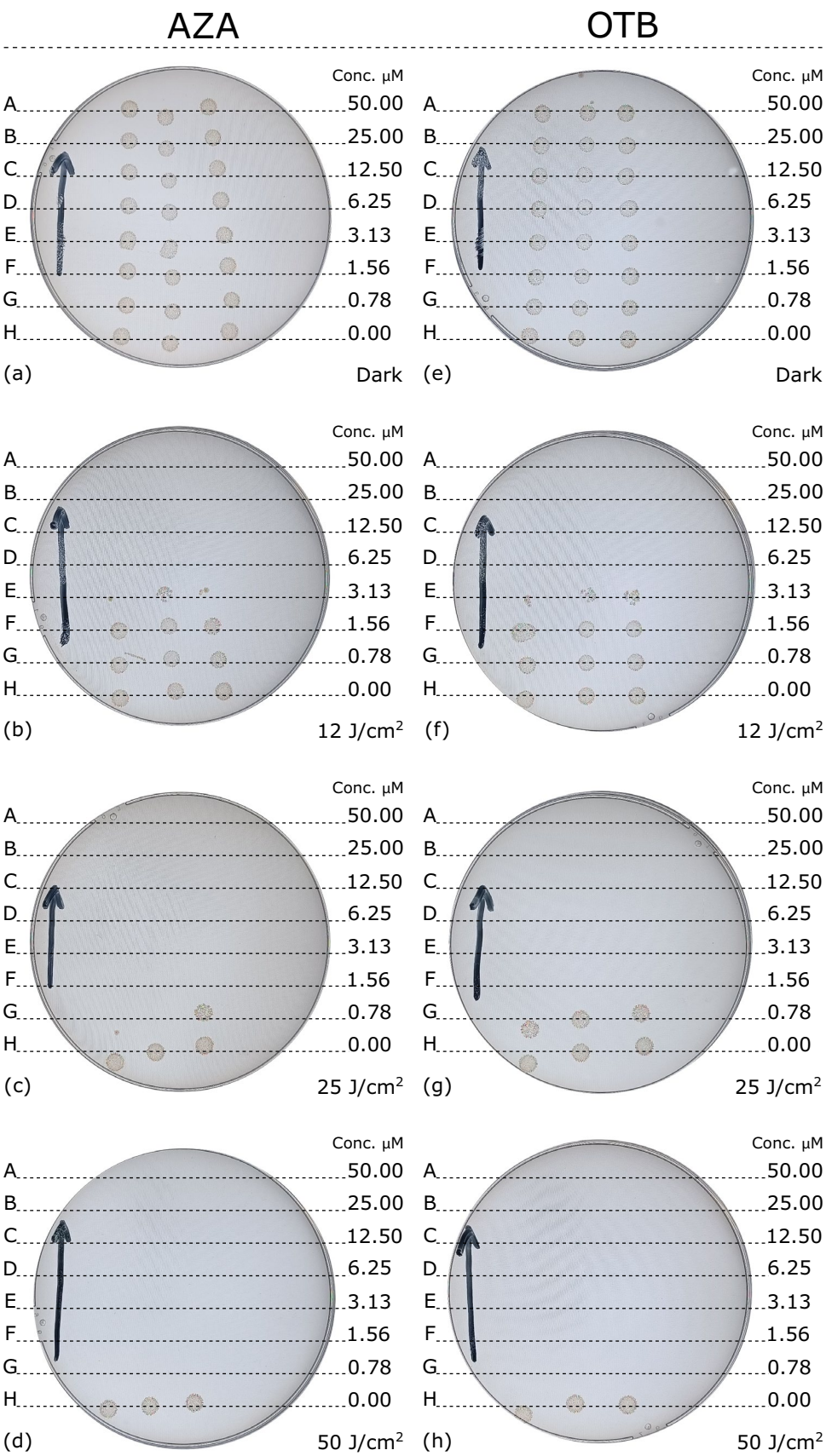

Fig. 8 Petri dishes that received aliquots containing 10^5 CFU/mL of *C. acnes* and different concentrations of AZA (a to d) and OTB (e to h) and that were exposed to different light exposure times that corresponded to optical fluence of 0, 12, 25 and 50 $\mathrm{J/cm^2}$. The arrows indicate the direction of concentration growth and the capital letters indicate from which wells the aliquots transferred to the Petri dish originated

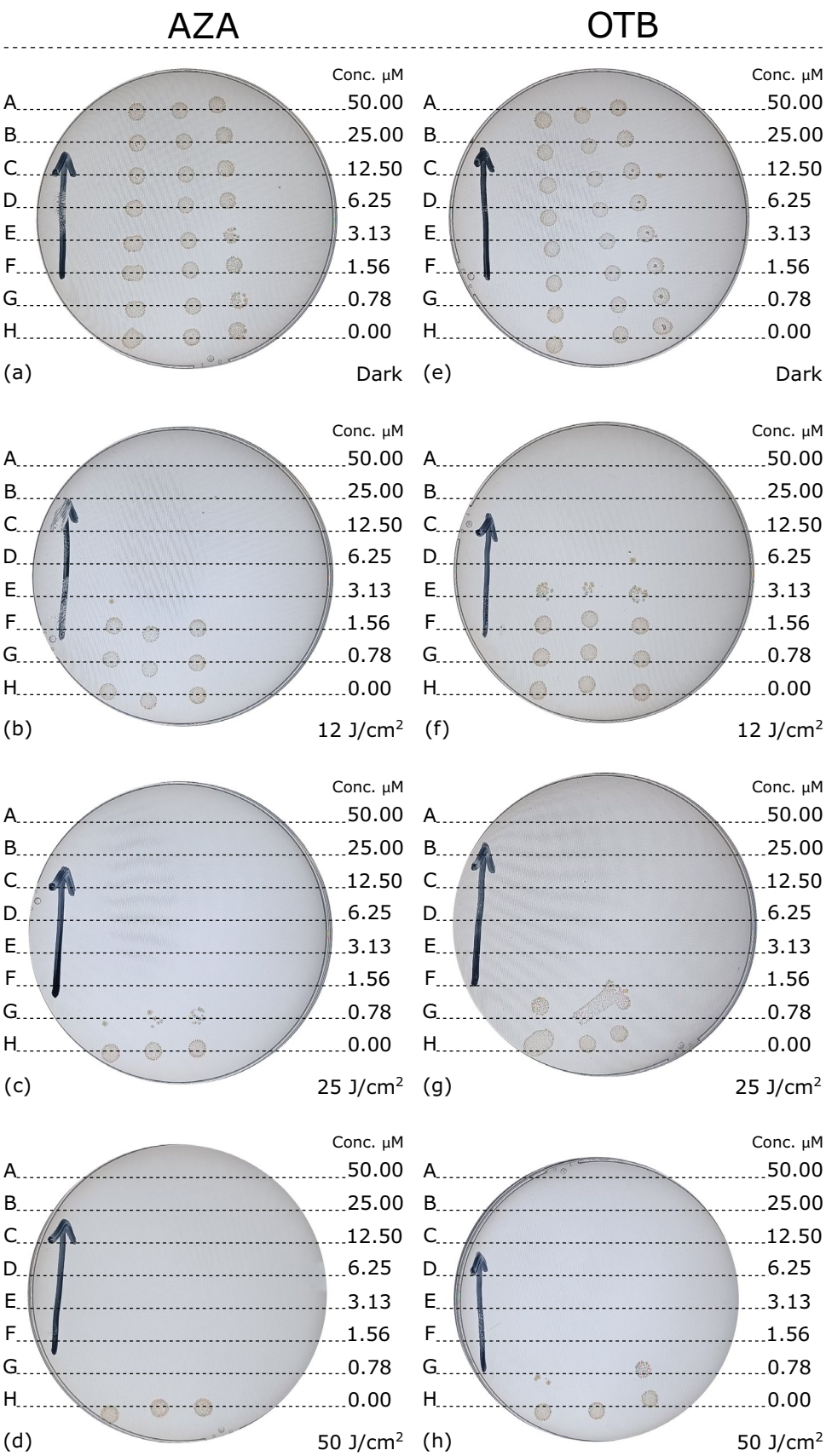

Fig. 9 Photographs of Petri dishes that received aliquots containing 10^5 CFU/mL of *S. epidermidis* and different concentrations of AZA (a to d) and OTB (e to h) and that were exposed to different light exposure times that corresponded to optical fluence of 0, 12, 25 and 50 $\mathrm{J/cm^2}$. The arrows indicate the direction of concentration growth and the capital letters indicate from which wells the aliquots transferred to the Petri dish originated

Table 1 Minimum bactericidal concentration (MBC) of Orthotoluidine blue (OTB) and azure A (AZA) for total inactivation of *S. epidermidis* and *C. acnes* under different optical fluence regimes. > 50.00 indicates that the MBC should be higher than the maximum concentration tested (50.00μM)

Optical fluence	Minimum bactericidal concentration (μM)			
J/cm^2	*C. acnes*		*S. epidermidis*	
	AZA	OTB	AZA	OTB
0	>50.00	>50.00	>50.00	>50.00
12	6.25	6.25	6.25	12.50
25	1.56	1.56	1.56	3.13
50	0.78	0.78	0.78	1.56

The absorbance spectra presented in Fig. 4a and b demonstrate that the presence of ABDA does not interfere with the optical properties of either PS. The lack of spectral overlap at 380 nm, where ABDA is monitored, together with its significantly higher absorbance compared to the PS at this wavelength, confirms the suitability of ABDA as a selective probe for singlet oxygen detection. Moreover, the absence of band shifts or distortions in the PS spectra upon addition of ABDA indicates that no aggregation or strong ground-state interactions occur under the experimental conditions. This validates the reliability of the assay for quantifying $^1O_2$ generation by both photosensitizers.

The systematic decay of ABDA absorbance at 380 nm observed in Figs. 5 and 6 confirms the continuous production of singlet oxygen ($^1O_2$) by both AZA and OTB under irradiation. The consistency of this behavior across different photosensitizer concentrations indicates that the generation of reactive oxygen species is sustained throughout the illumination period. Importantly, the absence of noticeable spectral changes or intensity loss in the absorption bands of the photosensitizers suggests that no significant photodegradation occurs under the applied irradiation conditions. This photostability is a critical feature for photodynamic applications, as it ensures reliable $^1O_2$ generation and preserves the optical properties of the photosensitizers during prolonged exposure to light.

ABDA reacts rapidly with singlet oxygen ($^1O_2$) to form its corresponding endoperoxide, leading to a decrease in its characteristic absorbance bands. Consequently, the decay rate of ABDA absorbance serves as an indirect measure of the rate of $^1O_2$ generation by the photosensitizer. It is important to note that this assay provides a kinetic indicator rather than an absolute quantitative determination of $^1O_2$ production [63]. The similar decay rates observed for AZA and OTB indicate comparable efficiencies in $^1O_2$ generation under the same irradiation conditions. The saturation behavior observed at concentrations above approximately 34 μM suggests the presence of limiting factors, such as reduced light penetration, self-shielding effects, or aggregation phenomena, which may constrain further increases in reactive oxygen species production at higher photosensitizer concentrations.

Although a deep investigation of the saturation in the ABDA decay rate is out the scope of this study, it is known that this type of phenomenon may be associated with the saturation of the photodynamic system, in which the increase in the concentration of PS does not imply an increase in the generation of $^1O_2$ due to limitations in available excitation light and molecular oxygen, and self-aggregation effects. As shown in Fig. 3e, above 17 μM dimerization begins to occur in both compounds, thus, the increase in the concentration of the dyes does not necessarily reflect in the increase in the concentration of the monomers, since dimerization begins to occur. It is recognized that dimerization affects the quantum yield of singlet oxygen due to the self-suppression of the excited states, which justifies the photodynamic saturation of the system from 34 μM .

4.3 Efficacy of in vitro aPDT

The absence of bactericidal activity in the dark control conditions demonstrates that neither AZA nor OTB exhibits intrinsic toxicity toward *C. acnes* within the tested concentration range. This result confirms that bacterial inactivation observed under illumination can be attributed exclusively to the photodynamic effect rather than to dark toxicity of the photosensitizers. Such behavior is a fundamental requirement for antimicrobial photodynamic therapy, as it ensures selectivity and safety by restricting bactericidal action to irradiated regions. The results shown in Fig. 8a and e therefore establish a reliable baseline for evaluating the light-dependent antimicrobial efficacy of both photosensitizers against *C. acnes*.

The results presented in Fig. 8 demonstrate that, for *C. acnes*, increasing optical fluence leads to a decrease in the photosensitizer concentration required to achieve complete bacterial inactivation, as reflected by the reduction in MBC values. This behavior is consistent with the expected dependence of antimicrobial photodynamic therapy on the total delivered light dose.

For *S. epidermidis* (Fig. 9), a similar trend is observed, with decreasing MBC values as optical fluence increases. However, in contrast to *C. acnes*, the MBC values differ between AZA and OTB, indicating distinct photodynamic efficiencies of the two photosensitizers against this bacterium. The lower MBC values obtained for AZA suggest a higher photodynamic effectiveness compared to OTB under the same irradiation conditions.

In both assays, the observation that bacterial growth persists in samples exposed to light in the absence of photosensitizer confirms that light alone is insufficient to induce bacterial inactivation. This reinforces that the observed

antimicrobial effects are attributable to the photodynamic action of the photosensitizers.

4.4 Overall discussion

UV-Vis spectroscopic analysis showed that the PS (AZA and OTB) have similar rates of absorption variation as a function of concentration and very close absorbance peaks, with good matching to the light source used.Despite good linearity, at concentrations above 17 $\mathrm{J/cm^2}$ the dimerization phenomenon occurs partially, however this phenomenon does not significantly harm singlet oxygen generation. Furthermore, according to the results obtained in the test with the ABDA probe, both PS have a similar singlet oxygen generation rate. Finally, and most relevantly, like OTB, AZA was able to photodynamically inactivate *C. acnes* and *S. epidermidis*, showing an MBC of 0.78 μM (50 $\mathrm{J/cm^2}$), which is two times lower than the MBC obtained when using OTB for aPDT of *S. epidermidis*. The results demonstrate that AZA is also a good candidate as PS for treating acne vulgaris and other infections associated with such microorganisms.

UV-Vis spectroscopic analyses demonstrated that the photosensitizers AZA and OTB exhibit similar absorption behaviors as a function of concentration, with absorbance peaks close together and well-matched to the light source used. Despite good linearity, partial dimerization is observed at doses above 17 μM, a phenomenon that does not significantly compromise the generation of singlet oxygen, which was similar for both compounds, as indicated by assays with the ABDA probe. Particularly relevant, AZA demonstrated high photodynamic efficiency in the inactivation of *C. acnes* and *S. epidermidis*, presenting a MBC of 0.78 μM under irradiation of 50 $\mathrm{J/cm^2}$, a value half that obtained with OTB in the aPDT of *S. epidermidis*. These results highlight the potential of AZA as a promising photosensitizer for treating acne vulgaris and skin infections associated with these microorganisms.

5 Conclusion

Based on these findings, future studies should focus on validating the efficacy and safety of AZA in more complex biological systems, including cellular, reconstructed skin, and in vivo models, as well as optimizing photodynamic parameters and developing topical formulations that promote its stability and follicular delivery. Furthermore, investigating its activity against bacterial biofilms, its impact on the skin microbiome, and its comparative performance with established photosensitizers will be essential to consolidate its therapeutic potential and enable its future clinical application in the management of acne vulgaris and other skin infections.

6 Limitations and future perspectives

Photodynamic inactivation assays were conducted under in vitro conditions, which do not fully capture the complexity of biological systems, including tissue barriers, immune responses, blood flow, and photosensitizer metabolism; therefore, the observed efficacy may not directly translate to in vivo settings. In addition, the use of a single light source with a fixed wavelength and a restricted optical fluence range limits the generalizability of photodynamic outcomes, as variations in irradiation parameters can significantly affect treatment efficiency. The absence of three-dimensional or biofilm-based models further restricts clinical relevance, particularly for acne, where microorganisms reside in structured biofilms and within the pilosebaceous unit. Ultimately, the evaluation of a limited number of microbial strains overlooks genetic diversity, intrinsic resistance mechanisms, and clinically relevant phenotypic variability.

Acknowledgements The authors thank the National Council for Scientific and Technological Development, processes: 200176/2024-2, 442004/2023-0, 420280-2023-5, 303635/2022-3, 301558/2022-1. This work was also supported by national funds from Fundação para a Ciência e Tecnologia (FCT/MCTES-PIDDAC) through the base funding UIDB/00690/2020 and UIDP/00690/2020; and from SusTEC, LA/P/0007/2020. L. B. Barros thanks FCT through the institutional scientific employment program–contract for her contract.

Author contributions L.S.H: Conceptualization, Writing - Original Draft, Writing - Review & Editing; C.T.M: Investigation; T.C.S.P.P: Investigation, Formal analysis, Visualization; C.C: Supervision; M.L.F: Writing - Review & Editing; L.C.M: Methodology; A.L.T: Resources, Writing - Review & Editing; J.A.S.A: Project administration, Writing - Review & Editing; L.B.B: Writing - Review & Editing, Resources, Funding acquisition.

Funding The Article Processing Charge (APC) for the publication of this research was funded by the Coordenação de Aperfeiçoamento de Pessoal de Nível Superior - Brasil (CAPES) (ROR identifier: 00x0ma614).

Data availability No datasets were generated or analysed during the current study.

Declarations

Conflict of Interest The authors have no relevant financial or non-financial interests to disclose. All authors certify that they have no affiliations with or involvement in any organization or entity with any financial interest or non-financial interest in the subject matter or materials discussed in this manuscript. The authors have no financial or proprietary interests in any material discussed in this article.

References

1. Dawson, A. L. & Dellavalle, R. P. Acne vulgaris. (2013) BMJ: British Medical Journal *346, Article f2634.*
2. Vasam, M., Korutla, S. & Bohara, R. A. (2023). Acne vulgaris: A review of the pathophysiology, treatment, and recent nanotechnology based advances. Biochemistry and Biophysics Reports *36, Article 101578.*
3. Reynolds, R. V., et al. (2024). Guidelines of care for the management of acne vulgaris. *Journal of the American Academy of Dermatology, 90*(1006), e1-1006.e30.
4. Morshed, A. S. et al. (2023) Understanding the impact of acne vulgaris and associated psychological distress on self-esteem and quality of life via regression modeling with cadi, dlqi, and who-qol. Scientific Reports *13, Article 21084.*
5. Stamu-O'Brien, C., Jafferany, M., Carniciu, S., & Abdelmaksoud, A. (2021). Psychodermatology of acne: Psychological aspects and effects of acne vulgaris. *Journal of Cosmetic Dermatology, 20*, 1080–1083.
6. Zouboulis, C. C., et al. (2005). What is the pathogenesis of acne? *Experimental Dermatology*, *14*, 143–152.
7. Hazarika, N. (2019). Acne vulgaris: new evidence in pathogenesis and future modalities of treatment. *Journal of Dermatological Treatment, 32*, 277–285.
8. Huang, T. Y., Jiang, Y. E., & Scott, D. A. (2022). Culturable bacteria in the entire acne lesion and short-chain fatty acid metabolites of cutibacterium acnes and staphylococcus epidermidis isolates. *Biochemical and Biophysical Research Communications, 622*, 45–49.
9. Mohammadi, M. (2025). Cutibacterium acnes bacteriophage therapy: exploring a new frontier in acne vulgaris treatment. *Archives of Dermatological Research, 317*, 84.
10. Hamann, T., et al. (2025). Distinct intraspecies variation of cutibacterium acnes and staphylococcus epidermidis in acne vulgaris and healthy skin. *Microorganisms, 13*, 299.
11. Lomholt, H. B., Scholz, C. F. P., Brüggemann, H., Tettelin, H., & Kilian, M. (2017). A comparative study of cutibacterium (propionibacterium) acnes clones from acne patients and healthy controls. *Anaerobe, 47*, 57–63.
12. Dagnelie, M.-A., Corvec, S., Timon-David, E., Khammari, A., & Dréno, B. (2022). Cutibacterium acnes and staphylococcus epidermidis: the unmissable modulators of skin inflammatory response. *Experimental Dermatology, 31*, 406–412.
13. Manurung, T. H. P., Sitohang, I. B. S., & Agustin, T. (2025). Staphylococcus caprae and staphylococcus epidermidis define the skin microbiome among different grades of acne vulgaris. *Archives of Dermatological Research, 317*, 156.
14. Ruchiatan, K., et al. (2023). Characteristics of biofilm-forming ability and antibiotic resistance of cutibacterium acnes and staphylococcus epidermidis from acne vulgaris patients. *Clinical, Cosmetic and Investigational Dermatology, 16*, 2457–2465.
15. Scott, E., Bullerjahn, G. S., & Burkhart, C. G. (2025). Targeting the cutibacterium acnes biofilm in acne. *International Journal of Dermatology*, *64*(6), 973. https://doi.org/10.1111/ijd.17752
16. Jain, S. (2004). Topical tretinoin or adapalene in acne vulgaris: an overview. *Journal of Dermatological Treatment, 15*, 200–207.
17. Kolli, S., Pecone, D., Pona, A., Cline, A., & Feldman, S. (2019). Topical retinoids in acne vulgaris: A systematic review. *American Journal of Clinical Dermatology, 20*, 345–365.
18. Cunliffe, W. J., Poncet, M., Loesche, C., & Verschoore, M. (1998). A comparison of the efficacy and tolerability of adapalene 0· 1% gel versus tretinoin 0· 025% gel in patients with acne vulgaris: a meta-analysis of five randomized trials. *British Journal of Dermatology, 139*(s52), 48–56.
19. Thiboutot, D., et al. (2007). Adapalene-benzoyl peroxide, a fixed-dose combination for the treatment of acne vulgaris: Results of a multicenter, randomized double-blind, controlled study. *Journal of the American Academy of Dermatology, 57*, 791–799.
20. Ochsendorf, F. (2015). Clindamycin phosphate 1.2%/tretinoin 0.025%: a novel fixed-dose combination treatment for acne vulgaris. *Journal of the European Academy of Dermatology and Venereology, 29*, 8–13.
21. Leung, A. K., Barankin, B., Lam, J. M., Leong, K. F. & Hon, K. L. (2020). Dermatology: How to manage acne vulgaris. Drugs in Context *10*.
22. Laux, B. (1989). Treatment of acne vulgaris. a comparison of doxycycline versus minocycline. *Hautarzt*, *40*, 577–581.
23. Rosso, J. D. D. (2015). Oral doxycycline in the management of acne vulgaris: Current perspectives on clinical use and recent findings with a new double-scored small tablet formulation. *The Journal of clinical and aesthetic dermatology, 8*, 19–26.
24. Hansted, B., & Reymann, F. (1982). Cyproterone acetate in the treatment of acne vulgaris in adult females. *Dermatologica, 164*, 117–126.
25. Fanta, D. (1990). Cyproterone acetate in acne. *Journal of Dermatological Treatment, 1*, S19–S22.
26. Lee, H.-S., Kim, I.-H. (2003). Salicylic acid peels for the treatment of acne vulgaris in asian patients. *Dermatologic Surgery, 29*, 1196–1199.
27. Magersan, S. E., Hancu, G. Rusu, A. (2023). A comprehensive bibliographic review concerning the efficacy of organic acids for chemical peels treating acne vulgaris. Molecules *28, Article 7219.*
28. Chen, X., Wang, S., Yang, M. Li, L. (2018). Chemical peels for acne vulgaris: a systematic review of randomised controlled trials. BMJ Open *8, Article e019607.*
29. Hongcharu, W., et al. (2000). Topical ala-photodynamic therapy for the treatment of acne vulgaris. *The Journal of investigative dermatology, 115*, 183–192.
30. Taylor, M., González, M. (2009). The practicalities of photodynamic therapy in acne vulgaris. British Journal of Dermatology *160*.
31. Sakamoto, F. H., Lopes, J. D., & Anderson, R. R. (2010). Photodynamic therapy for acne vulgaris: a critical review from basics to clinical practice: part I. Acne vulgaris: when and why consider photodynamic therapy? *Journal of the American Academy of Dermatology*, *63*(2), 183–193.
32. hong Huang, Q., Wang, D. Q., Zhou, B., & Luo, D. (2011). Photodynamic therapy of acne vulgaris. *International Journal of Dermatology and Venereology*, *37*, 343–345.
33. Qureshi, S., Rehan, Z., Ao, A., & Mukovozov, I. (2024). Photodynamic therapy in acne vulgaris: A systematic review. *Journal of Cutaneous Medicine and Surgery, 29*, 69–73.
34. Jean-Pierre, P., Tordjman, L., Ghodasara, A., et al. (2024). Emerging lasers and light-based therapies in the management of acne: A review. *Lasers in Medical Science, 39*, 245.

35. Singh, P. P., et al. (2024). Recent advancement in photosensitizers for photodynamic therapy. *Dyes and Pigments, 229*, Article 112262.
36. Henderson, B. W., & Dougherty, T. J. (1992). How does photodynamic therapy work? *Photochemistry and Photobiology, 55*, 145–157.
37. Dougherty, T. J., et al. (1998). Photodynamic therapy. *Journal of the National Cancer Institute, 90*, 889–905.
38. Castano, A. P., Demidova, T. N., & Hamblin, M. R. (2004). Mechanisms in photodynamic therapy: Part one - photosensitizers, photochemistry and cellular localization. *Photodiagnosis and Photodynamic Therapy, 1*, 279–293.
39. Zhou, Z., Song, J., Nie, L., & Chen, X. (2016). Reactive oxygen species generating systems meeting challenges of photodynamic cancer therapy. *Chemical Society Reviews, 45*, 6597–6626.
40. Zhou, W., Jiang, X., & Zhen, X. (2023). Development of organic photosensitizers for antimicrobial photodynamic therapy. *Biomaterials Science, 11*, 5108–5126.
41. Yerra, K. R., Soares, J. M., & Bagnato, V. S. (2025). The combined photosensitizers in antimicrobial photodynamic therapy: The case of methylene blue and photodithazine against klebsiella pneumoniae. *International Journal of Molecular Sciences, 26*, 10211.
42. Bhatia, N. (2023). The interventions to minimize pain during photodynamic therapy with 5-aminolevulinic acid for the treatment of cutaneous diseases. *Journal of Drugs in Dermatology, 22*, 1082–1087.
43. Zhang, Y., et al. (2024). Curcumin-mediated photodynamic therapy for mild to moderate acne: A self-controlled split-face randomized study. *Photodiagnosis and Photodynamic Therapy, 45*, Article 103887.
44. de Souza Crusca, J., de Moraes, L. H. O., Figueira, T. G., Parizotto, N. A. & Rodrigues, G. J. (2025). Photodynamic therapy effects with curcuma longa l. active ingredients in gel and blue led on acne: A randomized, controlled, and double-blind clinical study. Photonics *12, Article 80.*
45. Barroso, R. A., Navarro, R., Tim, C. R., et al. (2021). Antimicrobial photodynamic therapy against Propionibacterium acnes biofilms using hypericin (Hypericum perforatum) photosensitizer: in vitro study. *Lasers in Medical Science, 36*, 1235–1240.
46. Song, B. H., et al. (2014). Photodynamic therapy using chlorophyll-a in the treatment of acne vulgaris: A randomized, single-blind, split-face study. *Journal of the American Academy of Dermatology, 71*, 764–771.
47. Seo, H. M., et al. (2016). Effects of repetitive photodynamic therapy using indocyanine green for acne vulgaris. *International Journal of Dermatology, 55*, 1157–1163.
48. Jeon, Y. M., et al. (2015). Antimicrobial photodynamic therapy using chlorin e6 with halogen light for acne bacteria-induced inflammation. *Life Sciences, 124*, 56–63.
49. Soliman, M., Salah, M., Fadel, M., El-Lakkany, N., & Bassyouni, A. (2021). Contrasting the efficacy of pulsed dye laser and photodynamic methylene blue nanoemulgel therapy in treating acne vulgaris. *Archives of Dermatological Research, 313*, 173–180.
50. Moftah, N. H., Ibrahim, S. M., & Wahba, N. H. (2016). Intense pulsed light versus photodynamic therapy using liposomal methylene blue gel for the treatment of truncal acne vulgaris: a comparative randomized split body study. *Archives of Dermatological Research, 308*, 263–268.
51. Lee, Y.-D., et al. (2023). Topical methylene blue nanoformulation for the photodynamic therapy of acne vulgaris. *Archives of Dermatological Research, 315*, 885–893.
52. Zheng, Y., Yu, E., Weng, Q., et al. (2019). Optimization of hydrogel containing toluidine blue o for photodynamic therapy in treating acne. *Lasers in Medical Science, 34*, 1535–1545.
53. Shen, J. et al. (2019). In vitro effect of toluidine blue antimicrobial photodynamic chemotherapy on staphylococcus epidermidis and staphylococcus aureus isolated from ocular surface infection. Translational Vision Science and Technology *8, Article 45.*
54. Viola, G., Dall'acqua, F. (2006). Photosensitization of biomolecules by phenothiazine derivatives. *Current Drug Targets, 7*, 1135–1154.
55. Pluta, K., Morak-Młodawska, B., & Jeleń, M. (2011). Recent progress in biological activities of synthesized phenothiazines. *European journal of medicinal chemistry, 46*(8), 3179–3189.
56. Vara, J., Gualdesi, M. S., Bertolotti, S. G., & Ortiz, C. S. (2019). Two phenothiazine dyes as photosensitizers for the production of singlet oxygen. Photophysics, photochemistry and effects of aggregation. *Journal of Molecular Structure, 1181*, 1–7.
57. Vara, J., Gualdesi, M. S., Aiassa, V., Ortiz, C. S. (2019). Evaluation of physicochemical properties and bacterial photoinactivation of phenothiazine photosensitizers. *Photochemical & Photobiological Sciences, 18*, 1576–1589.
58. da Silva, A. C. P., et al. (2022). Application of chemometric method and computational analysis in the spectroscopic study of azure a dimerization. *Journal of Molecular Liquids, 366*, Article 120316.
59. Florence, N., & Naorem, H. (2014). Dimerization of methylene blue in aqueous and mixed aqueous organic solvent: A spectroscopic study. *Journal of Molecular Liquids, 198*, 255–258.
60. D'Ilario, L., & Martinelli, A. (2006). Toluidine blue: aggregation properties and structural aspects. *Modelling and Simulation in Materials Science and Engineering, 14*, 581.
61. de Souza, B. T. L., et al. (2021). The photosensitiser azure a disrupts mitochondrial bioenergetics through intrinsic and photodynamic effects. *Toxicology, 455*, Article 152766.
62. da Silva, A. C. P., et al. (2024). Functionalization of fibrous substrates with mesoporous silica nanoparticles as a strategy to obtain photodynamic antibacterial textiles. *Dyes and Pigments, 230*, Article 112342.
63. Entradas, T., Waldron, S., & Volk, M. (2020). The detection sensitivity of commonly used singlet oxygen probes in aqueous environments. *Journal of Photochemistry and Photobiology B: Biology, 204*, Article 111787.
64. Wang, Y., Lin, Y., He, S., Wu, S., & Yang, C. (2024). Singlet oxygen: Properties, generation, detection, and environmental applications. J HazardMater 461:132538. https://doi.org/10.1016/j.jhazmat.2023.132538
65. Francisco, C. M., et al. (2017). The photodynamic efficiency of phenothiazinium dyes is aggregation dependent. *New Journal of Chemistry, 41*, 14438–14443.